Communication

Sidelobe Suppression of Scanning Synthetic Beams Based on Coincidence Imaging Array Radar

Die Li, Mengran Zhao, Yiheng Nian, Ming Zhang, Lyu Lyu, Xiaoming Chen, Jianjia Yi, and Shitao Zhu

***Abstract*— Low sidelobe levels (SLLs) in scanning synthetic beams remain a problem for coincidence imaging array radar (CIAR) to achieve excellent anti-interference performance. In this communication, a sidelobe suppression method for the scanning synthetic beams is proposed. First, the fundamental model of the synthetic beam scanning method is presented with the introduction of the directional matching filter. Subsequently, the covariance matrix of the excitation signals is optimized using a convex optimization algorithm. This optimization allows for uniform bunching of the average power pattern within a specific angle range and simultaneous sidelobes' suppression of the scanning synthetic patterns. In addition to the partially correlated excitation signals without practical constraints, the excitation signals are synthesized using the alternating minimization algorithm when considering a constant modulus constraint. Finally, numerical simulations and experiments are conducted to validate the proposed sidelobe suppression method. The results demonstrate that the SLLs of the synthetic patterns with varying steering angles can be reduced to below −19.5 dB.**

***Index Terms*— Coincidence imaging array radar (CIAR), convex optimization, sidelobe suppression, synthetic beam scanning.**

I. Introduction

Radar high-resolution imaging exhibits significant application value in both military and civilian fields, including all-weather sea detection and imaging [1], sea disaster rescue [2], and ship navigation [3]. Traditional phased array radar can improve its range resolution by increasing the signal bandwidth, while its azimuth resolution is restricted by the aperture size [4]. To improve azimuth resolution, synthetic aperture radar [5] has been proposed whereby the radar aperture is increased through the collection of measurements along the relative motion between the radar and the target. Nevertheless, when synthetic aperture radar is applied in the forward-looking region, high resolution cannot be achieved due to the limited change in Doppler frequency gradient and azimuth ambiguity.

Recently, coincidence imaging array radar (CIAR), which can be considered as a type of multiple-input single-output (MISO) radar, has demonstrated its potential due to its advantages in staring imaging and super-resolution [6]. The CIAR concept is inspired by optical ghost imaging, which was first introduced by Pittman et al. [7]. Unlike a standard phased array that transmits identical signal waveforms, CIAR uses diverse signals to synthesize low-correlation radiation patterns. Considering the array similarity between multiple-input multiple-output (MIMO) radar [8] and CIAR, their mechanistic differences are compared here [9]. For transmitting waveforms, MIMO radar transmits orthogonal waveforms from each transmitter to ensure channel independence, while CIAR transmits time-independent and group orthogonal signals to produce randomly modulated detection modes in the imaging plane. In MIMO radar, the received signals from different transmitters are separated by exploiting the waveform orthogonality to gather target information from multiple paths or angles of observation. High resolution is achieved by a virtual extended array formed by convolution of transmitter and receiver locations. In CIAR, the imaging process depends on the correlation between received signals and detection modes, without separating echoes from different transmitters, and high resolution results from the spatial fluctuation of detection modes, which is the interference of transmitting waveforms.

In practical applications, one of the most challenging problems for CIAR is to determine the approximate area of targets to improve imaging efficiency. As a promising technique to overcome this challenge, beam scanning is a fundamental characteristic of radar systems and is essential for searching and tracking functions [10]. Nowadays, phased array [4] and frequency scanning antennas [11] are the primary methods used to achieve beam scanning. However, these methods are not well-suited for the CIAR system because it requires a large number of low-correlated radiation patterns to ensure imaging quality. In a recent study [12], we proposed an efficient method to simultaneously achieve super-resolution coincidence imaging and synthetic beam scanning based on a randomly excited antenna array. The steering angle of the scanning synthetic beam can be flexibly adjusted by modulating the excitation signals. However, the sidelobe levels (SLLs) of the scanning synthetic beams in [12] are high, which reduces the anti-interference capability of the CIAR system. Therefore, the SLLs should be reduced to a lower level to further improve the imaging performance.

Sidelobe suppression in classical arrays has been studied extensively, and several array synthesis algorithms have been reported for this purpose. Most of these algorithms use nonuniform amplitude tapers, including Taylor [13], binomial [14], Chebyshev [15], and other optimized distributions [16]. However, these traditional amplitude weighting methods are not suitable for CIAR due to the differences in the beam scanning basis between classical arrays and CIAR. In addition to the traditional methods, some optimization algorithms have also been used for sidelobe suppression, such as particle swarm optimizer [17], whale optimization algorithm [18], and convex optimization algorithm [19]. Among these optimization methods, the convex optimization algorithm shows higher speed and accuracy.

Received 21 October 2023; revised 6 October 2024; accepted 23 October 2024. Date of publication 12 November 2024; date of current version 17 January 2025. This work was supported in part by the Natural Science Foundation of China under Grant 62071371 and Grant 62471379, in part by the National Key Research and Development Program of China under Grant 2022YFB3902400, in part by the Foundation of National Key Laboratory of Electromagnetic Environment under Grant 202103014, and in part by the Aviation Science Foundation of China under Grant 20182007002. *(Corresponding author: Shitao Zhu.)*

Die Li, Yiheng Nian, Ming Zhang, Lyu Lyu, Xiaoming Chen, Jianjia Yi, and Shitao Zhu are with the School of Information and Communications Engineering, Xi'an Jiaotong University, Xi'an 710049, China (e-mail: shitaozhu@xjtu.edu.cn).

Mengran Zhao is with the School of Information and Communications Engineering, Xi'an Jiaotong University, Xi'an 710049, China, and also with the Institute of Electronics, Communication and Information Technology (ECIT), Queen's University Belfast, BT3 9DT Belfast, U.K.

Digital Object Identifier 10.1109/TAP.2024.3492501

The optimization problem discussed in this communication closely resembles that in [20]. In, three typical problems in MIMO radar, namely, maximum power design, beampattern matching design, and minimum sidelobe beampattern design, were addressed by Stoica et al. [20]. The purpose of minimum sidelobe beampattern design is to maximize the average power pattern in a given target direction with the desired half-power beamwidth, while minimizing the average power pattern in other directions. According to the radar equation, the detection range can be increased if the target directions are known. To address the scenario where the target directions are unknown, the minimax optimization is introduced in this communication. The optimization objective of this communication is to minimize the SLLs of the scanning synthetic beams while approximating the desired average power pattern. Compared with the minimum sidelobe beampattern design in [20], the optimization of scanning synthetic beams is proposed in this communication. The goal of SLL suppression for scanning synthetic beams is to improve the anti-interference capability of CIAR while maintaining its high-resolution characteristics [12]. Compared with [20], the main contributions of this communication are that the SLLs of scanning synthetic beams with various steering angles are suppressed simultaneously within a given angle range.

In this communication, an efficient method for the sidelobe suppression of scanning synthetic beams is proposed and analyzed. First, assisted by the directional matching filter, the mathematical model of the synthetic beam scanning method is presented. Second, the signal covariance matrix is optimized to bunch the average power pattern within a specific angle range and simultaneously suppress the sidelobes of the scanning synthetic patterns. Then, the excitation signals are synthesized without practical constraints and with a constant modulus constraint. Finally, numerical simulations and experiments are performed to validate the proposed sidelobe suppression method.

II. Model of Synthetic Beam Scanning

Since the low-correlated excitation signals are necessary for coincidence imaging, the radiation fields of the CIAR cannot cause spatial interference. This means that a pencil-shaped beam cannot be obtained directly. Synthetic beam scanning is an effective beam scanning method for the CIAR that can be achieved by postprocessing in the receiver.

Consider a uniform linear array with N elements positioned along the z-axis, serving as the transmitter of the CIAR, as illustrated in Fig. 1. The interelement spacing is d. Let $s_n(t)$ denote the complex signal transmitted by the nth element. The excitation signals of all the elements are stacked vertically together to form a vector-valued signal $\mathbf{s}(t) = [s_0(t), s_1(t), \ldots, s_{N-1}(t)]^{\mathrm{T}}$. It is assumed that there is no coupling between the antenna elements, and that the radiation pattern of each element is omnidirectional. Then the total field radiated by the array can be written as

$$y(t,\theta) = \sum_{n=0}^{N-1} s_n(t)\, e^{jkz_n \sin\theta} = \mathbf{a}^{\mathrm{T}}(\theta)\,\mathbf{s} \tag{1}$$

where k is the wavenumber, z_n is the position of the nth element with $z_n = [n-(N-1)/2]d$, θ is the angle between the observation direction and the normal direction of the array, and $\mathbf{a}(\theta)$ is the steering vector as follows:

$$\mathbf{a}(\theta) = \left[e^{jkz_0 \sin\theta}, e^{jkz_1 \sin\theta}, \ldots, e^{jkz_{N-1} \sin\theta}\right]^{\mathrm{T}}. \tag{2}$$

Define $\mathbf{R}$ as the covariance matrix of the excitation signals, where $\mathbf{R} = \langle \mathbf{s}(t)\mathbf{s}^H(t)\rangle$. The average power pattern of the CIAR can be represented as

$$P(\theta) = \langle |y(t,\theta)|^2 \rangle = \mathbf{a}^{\mathrm{T}}(\theta)\,\mathbf{R}\mathbf{a}^{*}(\theta). \tag{3}$$

The first-order correlation between the radiation field in one defined reference direction θ_r and that in an arbitrary direction θ can be given by

$$\chi(\theta,\theta_r) = \langle y(t,\theta)\, y^{*}(t,\theta_r)\rangle = \mathbf{a}^{\mathrm{T}}(\theta)\,\mathbf{R}\mathbf{a}^{*}(\theta_r). \tag{4}$$

When the excitation signals are time–space-independent, the average power pattern becomes omnidirectional, and the correlation pattern approximates a pencil-shaped pattern [6]. The maximum value of the correlation pattern is located in the reference direction. Therefore, when the received signals are processed according to the correlation function, the synthetic beam in the receiver is pencil-shaped, and its steering angle can be controlled by the parameter θ_r in (4). In fact, the postprocessing based on the correlation function is equivalent to a directional matching filter in the receiver. By increasing the number of directional matching filters, multiple synthetic beams with different steering angles can be generated simultaneously.

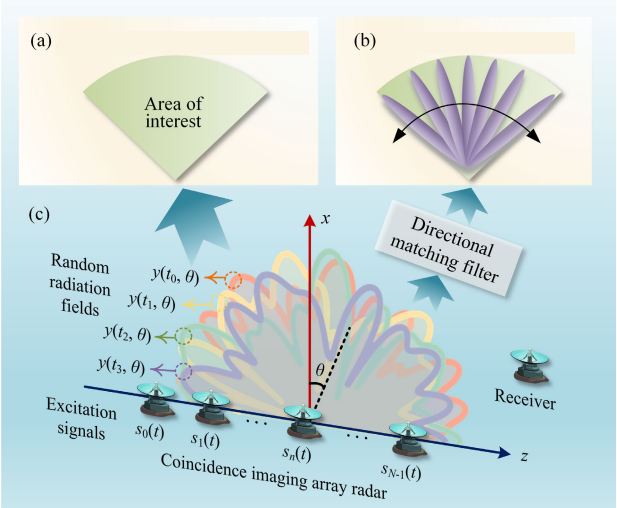

Fig. 1. Schematics of (a) average power pattern bunching, (b) synthetic beam scanning, and (c) CIAR system in the coordinate system.

III. Synthetic Pattern Design With Sidelobe Suppression

In this section, the covariance matrix of the excitation signals is optimized to bunch the average power pattern and simultaneously suppress the sidelobes of the synthetic beams, as illustrated in Fig. 1. Then, the excitation signals without constraint and with constant modulus constraint are synthesized based on the optimal covariance matrix.

A. Optimization of Signal Covariance Matrix

For classical CIAR, time–space-independent random signals are typically used as excitation signals. However, the time–space-independent signals result in a broad average power pattern, which leads to a low signal-to-noise ratio (SNR). The covariance matrix of the independent excitation signals is a diagonal matrix. To ensure the main lobe gain of the synthetic beam in the scanning regions, it is necessary to reinforce the average power pattern in the region of interest while suppressing it in other regions, as shown in Fig. 1(a). The desired average power pattern is a flat-top pattern, which means that the average power pattern should have a uniform value within

the detection spatial angle range, and should be below a certain level outside the detection spatial angle range.

In addition, an excellent synthetic scanning beam requires the generation of pencil-shaped synthetic patterns for each steering direction, as illustrated in Fig. 1(b). By minimizing the synthetic power in undesirable areas, the power scattered by jamming targets can be suppressed, potentially improving the anti-interference capability. The SLL of the synthetic beams generated by the CIAR is equivalent to that of the radiation pattern generated by the standard phased array with the same aperture size. Therefore, the objective of the optimization problem is to minimize the SLLs of the synthetic patterns using the minimax criterion.

The covariance matrix $\mathbf{R}$ must satisfy two indispensable constraints. The first constraint is that $\mathbf{R}$ must be a nonnegative matrix, since it is a covariance matrix by definition. The second constraint on $\mathbf{R}$ ensures that the total excitation power of all the elements is a constant. Mathematically, this is a maximin optimization problem with nonlinear constraints, which can be formulated as

$$\begin{aligned}
\min_{\mathbf{R}} \quad & \max_{\theta_m\in\Theta,\theta_i\in\Phi_m} \quad |\mathbf{a}^{\mathrm{T}}(\theta_i)\,\mathbf{R}\mathbf{a}^{*}(\theta_m)| \\
\text{s.t.} \quad & |\mathbf{a}^{\mathrm{T}}(\theta_m)\,\mathbf{R}\mathbf{a}^{*}(\theta_m) - U_0| \le \delta, \quad m = 1,\ldots,M \\
& |\mathbf{a}^{\mathrm{T}}(\theta_l)\,\mathbf{R}\mathbf{a}^{*}(\theta_l)| \le U_s, \quad l = 1,\ldots,L \\
& |\mathbf{a}^{\mathrm{T}}\left(\theta_m \pm \bar{B}_h/2\right)\mathbf{R}\mathbf{a}^{*}(\theta_m)| = U_0/2, \quad m = 1,\ldots,M \\
& \mathrm{Tr}(\mathbf{R}) = P_s \\
& \mathbf{R} \ge 0
\end{aligned} \tag{5}$$

where U_0 is the desired average power within the desired main lobe region, δ is the upper bound of the absolute error between the desired average power and the actual average power within the desired main lobe region, U_s is the sidelobe threshold of the average power pattern, $\bar{B}_h$ is the desired HPBW of the synthetic pattern, $\theta_m \in \Theta$, $m = 1,\ldots,M$ is a uniform grid of points covering the scanning regions of the synthetic pattern, $\theta_i \in \Phi_m$, $i = 1,\ldots,I$ is a uniform grid of points covering the sidelobe regions of the synthetic pattern, and $\theta_l \in \bar{\Theta}$, $l = 1,\ldots,L$ is a uniform grid of points covering the sidelobe regions of the average power pattern. The sidelobe regions of the synthetic pattern are defined as $\Phi_m = [-\pi/2, \theta_m - \bar{B}_0/2] \cup [\theta_m + \bar{B}_0/2, \pi/2]$, where $\bar{B}_0$ is the desired first-null beamwidth (FNBW) of the synthetic pattern. In particular, to maintain effective scanning, the main lobe regions of the average power pattern should be the same as the scanning regions of the synthetic pattern.

Based on array synthesis theory, the SLL of the synthetic beam obtained from the optimal covariance matrix is primarily determined by the desired HPBW and FNBW. The desired HPBW (FNBW) of the synthetic pattern can be determined based on the HPBW (FNBW) of the standard phased array with the same aperture size. Let B_h and B_0 be denoted as the HPBW and the FNBW of the radiation pattern of the standard phased array, respectively. To implement sidelobe suppression, the desired HPBW $\bar{B}_h$ and the desired FNBW $\bar{B}_0$ of the synthetic pattern are appropriately set to be less than B_h and B_0, respectively. The beamwidth factor κ is introduced to express the relationship between the desired HPBW (FNBW) and the HPBW (FNBW) of the standard phased array, as follows:

$$\bar{B}_0 = \kappa B_0, \quad \bar{B}_h = \kappa B_h. \tag{6}$$

The value range of the beamwidth factor κ is greater than 1. Since sidelobe suppression contributes to the increase in main lobe beamwidth, the optimal results of the scanning synthetic pattern are relative to the beamwidth factor. The relationship between the beamwidth factor and the SLLs of the scanning synthetic patterns will be studied in Section IV.

Algorithm 1 Alternating Minimization Algorithm

Input: Optimal covariance matrix $\mathbf{R}_{\mathrm{opt}} \in \mathbb{C}^{N\times N}$, $\mathbf{H} = \mathbf{R}_{\mathrm{opt}}^{1/2}$, sample number Q, element number N, excitation power of each element P_0

Output: Optimal signal waveform matrix $\mathbf{S} \in \mathbb{C}^{Q\times N}$, semiunitary matrix $\mathbf{U} \in \mathbb{C}^{Q\times N}$

Initialization: Generate $\mathbf{U}_0$ using (12);
$i \leftarrow 1$;
repeat
  Update $\mathbf{S}_i$: $\mathbf{S}_i \leftarrow \sqrt{P_0}e^{j\Phi}$, where $\Phi = arg(\mathbf{U}_i\mathbf{H})$;
  Update $\mathbf{U}_{i+1}$: $\mathbf{U}_{i+1} \leftarrow \tilde{\mathbf{U}}\tilde{\mathbf{V}}^H$, where $\tilde{\mathbf{U}}\Sigma\tilde{\mathbf{V}}^H$ is the singular value decomposition (SVD) of $\sqrt{Q}\mathbf{H}\mathbf{S}_i^H$;
  $i \leftarrow i + 1$;
until $\mathbf{U}_i$ *converged, i.e.,* $\|\mathbf{U}_i - \mathbf{U}_{i-1}\|^2 \le \epsilon$;
$\mathbf{S} = \sqrt{P_0}e^{j\Phi}$, where $\Phi = arg(\mathbf{U}_i\mathbf{H})$;
Return $\mathbf{S}$.

Consider two distinct vectors $\mathbf{x}_1$ and $\mathbf{x}_2$, along with a matrix $\mathbf{C}$. These three variables satisfy the following property:

$$\mathbf{x}_1^{\mathrm{T}}\mathbf{C}\mathbf{x}_2^{*} = \mathrm{Tr}\left(\mathbf{x}_1^{*}\mathbf{x}_2^{\mathrm{T}}\mathbf{C}\right) \tag{7}$$

where $\mathrm{Tr}(\cdot)$ donates the trace of matrix. To simplify the expression in (5), an auxiliary matrix $\mathbf{A}$ is introduced as follows:

$$\mathbf{A}(\theta_1,\theta_2) = \mathbf{a}^{*}(\theta_1)\,\mathbf{a}^{\mathrm{T}}(\theta_2). \tag{8}$$

According to (7) and (8), the matrix product terms related to the covariance matrix $\mathbf{R}$ in (5) can be expressed in matrix trace form. Furthermore, an auxiliary variable σ ($\sigma > 0$) is introduced to transform the maximin optimization problem into a minimization problem with additional inequality constraints. Accordingly, (5) can be equivalently expressed as

$$\begin{aligned}
\min_{\mathbf{R}} \quad & \sigma \\
\text{s.t.} \quad & |\mathrm{Tr}\{\mathbf{A}(\theta_m,\theta_m)\,\mathbf{R}\} - U_0| \le \delta, \quad m = 1,\ldots,M \\
& |\mathrm{Tr}\{\mathbf{A}(\theta_l,\theta_l)\,\mathbf{R}\}| \le U_s, \quad l = 1,\ldots,L \\
& |\mathrm{Tr}\{\mathbf{A}(\theta_i,\theta_m)\,\mathbf{R}\}| \le \sigma, \quad i = 1,\ldots,I \\
& \qquad\qquad\qquad\qquad m = 1,\ldots,M \\
& |\mathrm{Tr}\left\{\mathbf{A}\left(\theta_m \pm \bar{B}_h/2,\theta_m\right)\mathbf{R}\right\}| = U_0/2, \quad m = 1,\ldots,M \\
& \mathrm{Tr}(\mathbf{R}) = P_s \\
& \mathbf{R} \ge 0.
\end{aligned} \tag{9}$$

In (9), the objective function and all other constraints exhibit convexity with respect to $\mathbf{R}$. Problem (9) can be viewed as an instance of semidefinite programming [21], which is a form of linear programming. Since semidefinite programming is a special case of convex optimization, (9) can be solved efficiently using convex optimization algorithms. Once the optimal covariance matrix $\mathbf{R}_{\mathrm{opt}}$ is determined, an excitation signal sequence $\mathbf{s}(t)$ that satisfies the optimal covariance matrix must be further synthesized.

B. Signal Synthesis Without Constraint

Define the signal waveform matrix as $\mathbf{S} \in \mathbb{C}^{Q\times N}$, where Q represents the sample number in each signal waveform. The nth column of the signal waveform matrix represents the transmitted waveform of the nth array element. The sample covariance matrix can then be expressed as

$$\hat{\mathbf{R}} = \frac{1}{Q}\mathbf{S}^H\mathbf{S}. \tag{10}$$

The number of unknowns in the covariance matrix $\mathbf{R}$ is N^2, while the number of unknowns in the signal waveform matrix $\mathbf{S}$ is NQ. Therefore, an auxiliary matrix should be introduced to recover the signal waveform matrix from the optimal covariance matrix. Without considering practical constraints, the signal waveform matrix satisfying a given covariance matrix $\mathbf{R}$ can be written as

$$\mathbf{S} = \sqrt{Q}\mathbf{U}\mathbf{R}_{\text{opt}}^{1/2} = \sqrt{Q}\mathbf{U}\mathbf{H} \tag{11}$$

where $\mathbf{U} \in \mathbb{C}^{Q\times N}$ is an arbitrary semiunitary matrix, and $\mathbf{H} \in \mathbb{C}^{N\times N}$ is the Cholesky factor matrix of the optimal covariance matrix $\mathbf{R}_{\text{opt}}$. To guarantee $\mathbf{U}^H\mathbf{U} = \mathbf{I}$, the semiunitary matrix $\mathbf{U}$ can be obtained by

$$\mathbf{U} = \mathbf{U}_w\mathbf{V}_w^H \tag{12}$$

with

$$\mathbf{W} = \mathbf{U}_w\Sigma_w\mathbf{V}_w^H \tag{13}$$

where each column of $\mathbf{W}$ represents an independent and identically distributed normal random vector with mean zero and covariance matrix $\mathbf{I}$, and $\mathbf{U}_w$, Σ_w, and $\mathbf{V}_w$ are the SVD factors of $\mathbf{W}$. Without considering practical constraints, the sample covariance matrix is equal to the optimal covariance matrix when the sample number is greater than the element number.

C. Signal Synthesis With Constant Modulus Constraint

In radar systems, to avoid expensive amplifiers and analog-to-digital converters, it is typically necessary to maintain a constant modulus for the excitation signals. The solution process for the signal waveform matrix with a constant modulus constraint involves two key steps. First, the excitation power constraint with $\mathbf{R}_{nn} = P_0$ should be incorporated into (9), where P_0 represents the excitation power of each element, and can be defined as $P_0 = P_s/N$. Due to the convexity of the excitation power constraint, (9) remains amenable to solution by convex optimization algorithms. Then, the constant modulus constraint, where $|s_n(t)| = \sqrt{P_0}$, should be taken into account during signal synthesis process based on the optimal covariance matrix.

Based on the theoretical foundation of excitation signal synthesis without constraints, the problem of signal synthesis with constant modulus constraint can be described as follows:

$$\begin{aligned} &\min_{\mathbf{S};\mathbf{U}} \ \|\mathbf{S} - \sqrt{Q}\mathbf{U}\mathbf{H}\|^2 \\ &\text{s.t.} \ \ |s_n(t)| = \sqrt{P_0}, \quad n = 0, \ldots, N-1 \\ &\qquad \mathbf{U}^H\mathbf{U} = \mathbf{I}. \end{aligned} \tag{14}$$

The minimization problem in (14) is nonconvex due to the nonconvexity of the constraint $\mathbf{U}^H\mathbf{U} = \mathbf{I}$. Here, the alternating minimization algorithm is used to solve (14). The algorithm procedure for the alternating minimization algorithm is outlined in Algorithm 1.

For the proposed synthetic beam scanning method, the transmitting signals of the CIAR can be designed in advance based on the application requirements. The expected scanning regions are divided into a number of subregions, each with a size of half-power beamwidth, where each subregion corresponds to a synthetic beam with a steering angle determined by the center of that subregion. Once the array structure and scanning region are established, the transmitting signals can be optimized to simultaneously suppress the SLLs of the synthetic beams with the desired steering angles. Since the average power pattern within the scanning regions of the synthetic beams is constrained in the optimization problem, all the target information within these regions is captured in the echo signals. By processing the echo signals with the designed directional matching filter, the synthetic beam scanning in the desired regions can be achieved simultaneously. Therefore, the real-time processing performance of the proposed synthetic beam scanning method is equivalent to multibeam scanning of conventional radar.

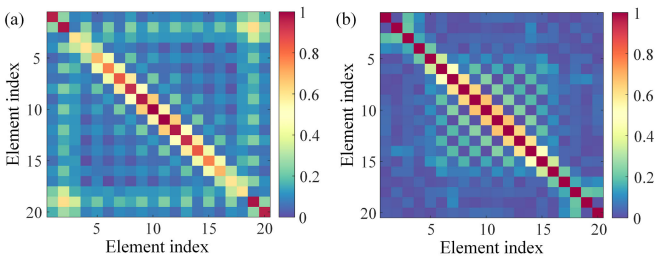

Fig. 2. Normalized optimal signal covariance matrices. (a) Without constraint and (b) with constant modulus constraint.

IV. Simulations and Experiments

To validate the performance of the proposed sidelobe suppression method, simulations and experiments are performed in this section. The transmitter of the considered CIAR consists of a uniform linear array of $N = 20$ antenna elements, where the distance between adjacent elements is half-wavelength, i.e., $d = \lambda_c/2$. Without loss of generality, the total excitation power is set to $P_s = 1$ W. In the numerical experiments, the scanning region is taken as $\Theta = [-30°, 30°]$ with the number of uniform samples as $M = 20$. The regions outside of the scanning region are taken as $\bar{\Theta} = [-90°, -30°] \cup [30°, 90°]$ with the number of uniform sampling points as $L = 40$. The sidelobe regions of the synthetic pattern are taken as $\Phi_m = [-90°, \theta_m - \bar{B}_0/2] \cup [\theta_m + \bar{B}_0/2, 90°]$ with the number of uniform samples as $I = 60$.

In (9), the upper bound of the error between the desired average power and the actual average power within the main lobe region of the average power pattern is set to an empirical value of $\delta = 0.01$. Considering the opposite relationship between the SLL of the average power pattern and that of the synthetic pattern, the sidelobe threshold of the average power pattern is set to $U_s = 0.3$ to achieve better performance of synthetic sidelobe suppression. The sample number is set to 30. In the simulations, the optimal covariance matrix can be obtained by solving (9) using the convex optimization algorithm.

To validate the effectiveness of the proposed methods, the simulation results of signal synthesis without constraint and with a constant modulus constraint are presented. When the beamwidth factor is set to 1.4, the normalized optimal covariance matrices in the two cases are depicted in Fig. 2. It can be observed that the covariance matrix with a constant modulus constraint exhibits a more uniform distribution than the one without constraint. In the former case, the sample covariance matrix is equal to the optimal covariance matrix when the sample number exceeds the element number, according to (11). In the latter case, due to the constraint imposed by the constant modulus, some inevitable errors may arise between the optimal covariance matrix and the sample covariance matrix. The radiation gain patterns of six samples obtained from the optimal constant modulus signals, which are randomly selected from the total sample set, are presented in Fig. 3(a).

The comparison between the average power gain patterns of the independent signals and those of the optimal signals in the two cases is shown in Fig. 3(b). The average power gain of the independent signals is 0 dB, while the average power gains of the optimized signals in the two cases are 1.94 and 1.85 dB, respectively. From Fig. 3(b), it can be observed that the average power distributions are nearly uniform within the desired angle range of 60° in the two cases. The fluctuations of the average power gains within the main lobe region in the two cases are about 0.52 and 0.1 dB, respectively.

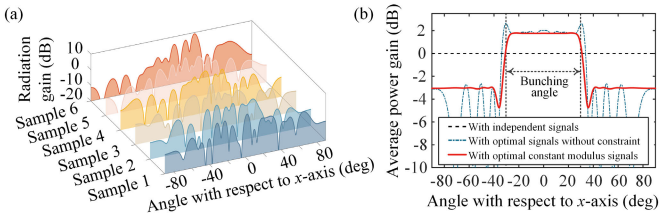

Fig. 3. (a) Radiation gain patterns of six randomly selected samples obtained from the optimal constant modulus signals and (b) average power patterns obtained from independent signals, optimal signals without constraint, and optimal constant modulus signals.

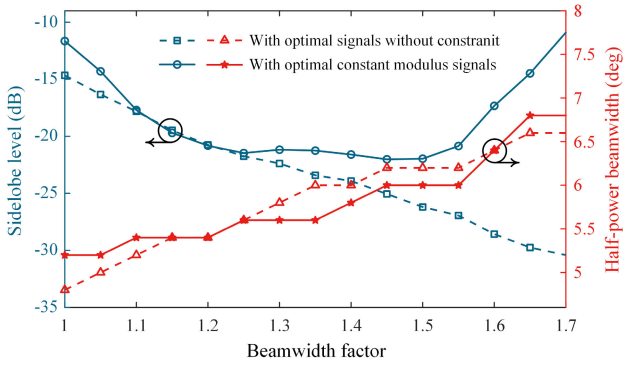

Fig. 4. SLLs and HPBWs of the scanning synthetic beams for different beamwidth factors in the two cases.

The SLLs of the optimal average power pattern in the two cases are −4.95 and −4.86 dB, respectively. These results clearly demonstrate that the average power bunchings in the two cases have significantly enhanced the gain of the CIAR, and the average power pattern of the optimal constant modulus signals is smoother than that of the optimal signals without constraint.

Since sidelobe suppression contributes to the increase in the main lobe beamwidth, the optimal results of the scanning synthetic pattern are relative to the beamwidth factor. To illustrate the influence of the beamwidth factor on sidelobe suppression of the scanning synthetic beams, the maximum SLLs of the scanning synthetic beams and the HPBWs of the synthetic beam with the steering angle of 0° for different beamwidth factors are shown in Fig. 4. As the beamwidth factor increases, the SLL of the scanning synthetic beams without constraint decreases, while that of the scanning synthetic beams with constant modulus constraint first decreases and then increases. In engineering applications, to control the impact on the main lobe performance, the increase in HPBW caused by sidelobe suppression should usually not exceed 20% of the HPBW without sidelobe suppression. The HPBW and SLL of the synthetic beam with the independent signals are 5.0° and −13.19 dB, respectively. Therefore, the HPBW of the optimal synthetic beam is set to 6.0°. According to Fig. 4, the beamwidth factor for signal synthesis without constraint should not exceed 1.4, and the beamwidth factor for signal synthesis with constant modulus constraint should not exceed 1.45.

When the beamwidth factor is set to 1.45, the scanning synthetic patterns obtained from the optimal signal sequences with six different steering angles of ±5°, ±15°, and ±25° are presented in Fig. 5. The synthetic gains for these six cases are 12.61, 12.65, 12.61, 12.61, 12.65, and 12.61 dB, respectively. The SLLs of the synthetic patterns are −23.31, −22.60, −22.23, −22.23, −22.60, and −23.31 dB, respectively. To further illustrate the effect of the proposed sidelobe suppression method, the synthetic gain patterns of the independent signals, the optimal signals without constraint, and the optimal

TABLE I
PARAMETERS OF SYNTHETIC PATTERNS FOR THREE SIGNAL CLASSES

Signal class	Synthetic gain	HPBW	SLL
Independent signals	13.01 dB	5.0°	−13.19 dB
Optimal signals without constraint	12.51 dB	6.0°	−25.53 dB
Optimal constant modulus signals	12.57 dB	6.0°	−22.23 dB

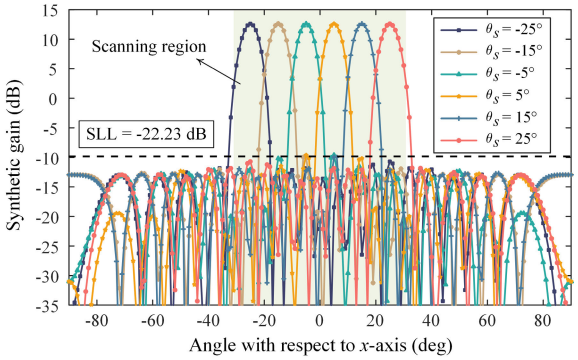

Fig. 5. Scanning synthetic patterns obtained from the optimal constant modulus signals when the steering angles are ±5°, ±15°, and ±25°, respectively.

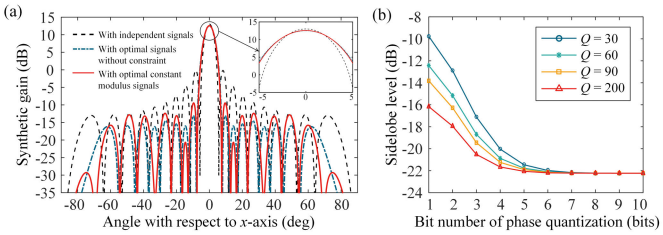

Fig. 6. (a) Synthetic gain patterns of the independent signals, the optimal signals without constraint, and the optimal constant modulus signals when the steering angle is 0°. (b) SLL curves with different bit numbers of phase quantization when the sample numbers are 30, 60, 90, and 200, respectively.

constant modulus signals when the steering angle is 0° are shown in Fig. 6(a). The synthetic gains, HPBWs, and SLLs of the synthetic patterns in the three cases are listed in Table I. It can be observed that the synthetic SLL with the optimal signals decreases by 12.34 dB compared with the independent signals, while the synthetic SLL with the optimal constant modulus signals decreases by 8.83 dB compared with the independent signals.

In practical applications with digital phase shifters, it is imperative to account for phase quantization errors. The impact of these errors on SLLs has been investigated through 1000 Monte Carlo trials. The SLL curves with different bit numbers of phase quantization are depicted in Fig. 6(b) when the sampling numbers are 30, 60, 90, and 200, respectively. From the results, it can be observed that the SLL of the scanning synthetic patterns can be suppressed below −20 dB when the bit number of phase quantization is greater than 4 bits, which demonstrates excellent engineering application capabilities. In addition, as the sample number increases, the impact of phase quantization errors on the SLL of the scanning synthetic patterns decreases.

To verify the effectiveness of the proposed sidelobe suppression method, an experiment is designed as shown in Fig. 7. A total of 20 pyramidal horn antennas are used as transmitters in the CIAR. The distance between adjacent transmitters is half the free-space

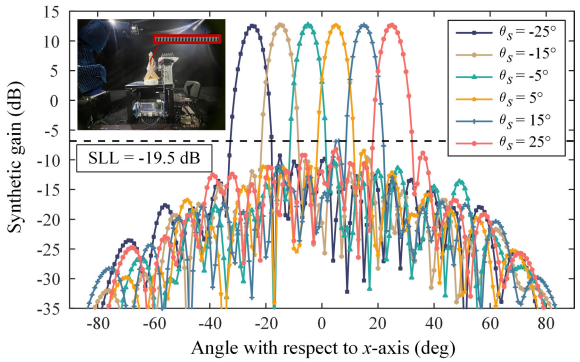

Fig. 7. Experimental scanning synthetic patterns for the steering angles of ±5°, ±15°, and ±25°, respectively.

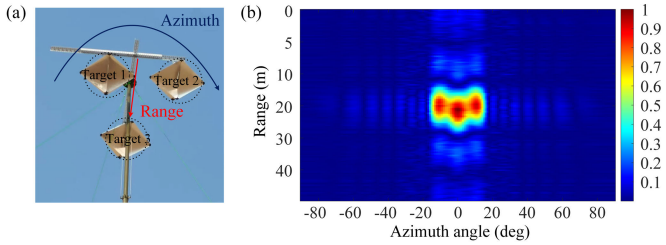

Fig. 8. (a) Real targets and (b) measured imaging results when the transmitting signals are optimal constant modulus signals.

wavelength at 10 GHz. The sample number in the time domain is set to 30. The excitation signals of the transmitters are set to the optimal constant modulus signal sequences when the beamwidth factor is 1.45. The digital phase shifter uses 6-bit quantization accuracy. The far-field data of the transmitters in the CIAR are measured in the anechoic chamber. According to the measured far-field data, the scanning synthetic patterns are calculated for the steering angles of ±5°, ±15°, and ±25°, as shown in Fig. 7. The SLL of the scanning synthetic patterns is −19.5 dB. Comparing Figs. 5 and 7, it can be concluded that the experimental and numerical results are comparable. The decrease in the experimental SLL can be attributed to excitation errors and environmental factors.

To validate the effectiveness of the proposed synthetic beam scanning method in the CIAR, a three-target imaging experiment was performed with the CIAR. The distances between the three targets and the CIAR are approximately $2000\lambda_c$, with azimuth angles of −10°, 0°, and 10°, respectively. As shown in Fig. 8(a), the ranges of targets 1 and 2 are closer than that of target 3. When the transmitting signals are optimal constant modulus signals, the measured imaging results are obtained by processing the echo signals with the designed directional matching filter, as shown in Fig. 8(b). It can be illustrated that the multiple targets in different directions can be efficiently located by the synthetic beam scanning method.

V. Conclusion

In this communication, a sidelobe suppression method for the scanning synthetic beams based on CIAR was proposed. First, the fundamental signal model and the synthetic beam scanning method were presented. Then, the joint optimization method was used to obtain the covariance matrix of the excitation signals. Accordingly, the partially correlated excitation signals without practical constraints and with constant modulus constraint were derived. Finally, numerical simulations and experiments were conducted to validate the proposed sidelobe suppression method. It was demonstrated that the sidelobes of the synthetic patterns with varying steering angles could be suppressed to below −19.5 dB while considering a constant modulus constraint of the excitation signals. In summary, the proposed method showed promising potentials in improving the performance of synthetic scanning beams and enhancing the anti-interference capability of CIAR systems.

References

[1] L.-L. Fu, *Seasat Views Oceans and Sea Ice With Synthetic-aperture Radar*, vol. 81. Pasadena, CA, USA: California Institute of Technology, 1982.
[2] J. Harlan et al., "The integrated ocean observing system high-frequency radar network: Status and local, regional, and national applications," *Mar. Technol. Soc. J.*, vol. 44, no. 6, pp. 122–132, Nov. 2010.
[3] Y. Huang, P. V. Brennan, D. Patrick, I. Weller, P. Roberts, and K. Hughes, "FMCW based MIMO imaging radar for maritime navigation," *Prog. Electromagn. Res.*, vol. 115, pp. 327–342, 2011.
[4] R. J. Mailloux, *Phased Array Antenna Handbook*. Norwood, MA, USA: Artech House, 2017.
[5] M. Soumekh, *Synthetic Aperture Radar Signal Processing*, vol. 7. New York, NY, USA: Wiley, 1999.
[6] S. Zhu, A. Zhang, Z. Xu, and X. Dong, "Radar coincidence imaging with random microwave source," *IEEE Antennas Wireless Propag. Lett.*, vol. 14, pp. 1239–1242, 2015.
[7] T. B. Pittman, Y. H. Shih, D. V. Strekalov, and A. V. Sergienko, "Optical imaging by means of two-photon quantum entanglement," *Phys. Rev. A, Gen. Phys.*, vol. 52, no. 5, p. R3429, Nov. 1995.
[8] A. Haimovich, R. Blum, and L. Cimini, "MIMO radar with widely separated antennas," *IEEE Signal Process. Mag.*, vol. 25, no. 1, pp. 116–129, Dec. 2007.
[9] D. Li, X. Li, Y. Qin, Y. Cheng, and H. Wang, "Radar coincidence imaging: An instantaneous imaging technique with stochastic signals," *IEEE Trans. Geosci. Remote Sens.*, vol. 52, no. 4, pp. 2261–2277, Apr. 2014.
[10] M. A. Richards, J. Scheer, W. A. Holm, and W. L. Melvin, *Principles of Modern Radar*, vol. 1. Princeton, NJ, USA: Citeseer, 2010.
[11] A. Sarkar, A. Sharma, A. Biswas, and M. J. Akhtar, "Compact CRLH leaky-wave antenna using TE_{20}-mode substrate-integrated waveguide for broad space radiation coverage," *IEEE Trans. Antennas Propag.*, vol. 68, no. 10, pp. 7202–7207, Oct. 2020.
[12] D. Li et al., "Synthetic beam scanning and super-resolution coincidence imaging based on randomly excited antenna array," *IEEE Trans. Geosci. Remote Sens.*, vol. 61, 2023, Art. no. 2002414.
[13] A. Villeneuve, "Taylor patterns for discrete arrays," *IEEE Trans. Antennas Propag.*, vol. AP-32, no. 10, pp. 1089–1093, Oct. 1984.
[14] R. Chopra and G. Kumar, "Series-fed binomial microstrip arrays for extremely low sidelobe level," *IEEE Trans. Antennas Propag.*, vol. 67, no. 6, pp. 4275–4279, Jun. 2019.
[15] G. T. F. de Abreu and R. Kohno, "A modified Dolph-Chebyshev approach for the synthesis of low sidelobe beampatterns with adjustable beamwidth," *IEEE Trans. Antennas Propag.*, vol. 51, no. 10, pp. 3014–3017, Oct. 2003.
[16] K. Guney and S. Basbug, "'Interference suppression of linear antenna arrays by amplitude-only control using a bacterial foraging algorithm," *Prog. Electromagn. Res.*, vol. 79, pp. 475–497, 2008.
[17] S. K. Goudos, V. Moysiadou, T. Samaras, K. Siakavara, and J. N. Sahalos, "Application of a comprehensive learning particle swarm optimizer to unequally spaced linear array synthesis with sidelobe level suppression and null control," *IEEE Antennas Wireless Propag. Lett.*, vol. 9, pp. 125–129, 2010.
[18] C. Zhang, X. Fu, L. P. Ligthart, S. Peng, and M. Xie, "Synthesis of broadside linear aperiodic arrays with sidelobe suppression and null steering using whale optimization algorithm," *IEEE Antennas Wireless Propag. Lett.*, vol. 17, pp. 347–350, 2018.
[19] C. Yang et al., "Pattern synthesis algorithm for range ambiguity suppression in the LT-1 mission via sequential convex optimizations," *IEEE Trans. Geosci. Remote Sens.*, vol. 60, 2021, Art. no. 2001713.
[20] P. Stoica, J. Li, and Y. Xie, "On probing signal design for MIMO radar," *IEEE Trans. Signal Process.*, vol. 55, no. 8, pp. 4151–4161, Aug. 2007.
[21] H. Wolkowicz, R. Saigal, and L. Vandenberghe, *Handbook of Semidefinite Programming: Theory, Algorithms, and Applications*, vol. 27. Springer, 2012.